13th ewtec 2019 Proceedings of the 13th European Wave and Tidal Energy Conference 1-6 Sept 2019, Naples, Italy

Experimental and numerical analysis of GEMSTAR, a tethered tidal current energy harvester

Domenico P. Coiro, Giancarlo Troise, Nadia Bizzarrini and Guido Lazzerini

***Abstract*—This work describes the patented tethered system GEMSTAR for the exploitation of tidal stream energy. Tidal currents represent a valuable energy source, where available, mainly due to their repetitive and predictable behaviour, which allows reliable energy production estimations. The GEMSTAR system is composed of two hydrokinetic turbines supported by a floating structure. The device is tethered to the seabed by means of a flexible mooring cable, which allows the alignment to the flow direction according to the tidal stream inversions. The main results of the numerical and experimental investigations performed on the system at the University of Naples will be presented, together with further developments of the project, in particular with respect to the redesign of the hydrokinetic turbine blade requested by the new power control strategy adopted.**

***Keywords*—hydrokinetic turbines, tidal stream energy, floating horizontal axis turbines, tethered system.**

I. INTRODUCTION

THE GEMSTAR (Generatore Elettrico Marino, Sustainable Tethered Advanced Rotors) system is a floating hydrokinetic energy converter, especially suitable for tidal energy exploitation, provided with two horizontal-axis turbines and tethered to the seabed by means of a flexible mooring cable. The GEMSTAR is an innovative system developed over several years of applied research at the University of Naples in cooperation with the research consortium SEAPOWER. It represents the evolution of the first prototype GEM, The Ocean Kite, developed since 2005 and tested in a real sea environment in 2012. The GEMSTAR essentially comprises a submerged floating body with a streamlined hydrodynamic shape, tailfins improving its static and dynamic stability, and two hydrokinetic turbines, symmetrically mounted on both sides of the main floating body, acting as prime movers for two electrical generators.

Thanks to its mooring system, the GEMSTAR can be lowered at its operating depth and risen to the water surface for periodic maintenance operations, simply releasing the mooring cable. Besides, the system is characterised by a stable behaviour in operating conditions, and it can align itself with the different flow directions just rotating around a single anchoring point. Thanks to its design, it is also easily transportable and it needs a short time to be deployed and recovered for maintenance purposes. These advantages can drastically reduce operation and maintenance costs. An illustration of the GEMSTAR system is reported in Fig. 1.

A review of the main results of the GEMSTAR project development will be presented in this work. Previous research activities have involved several experimental and numerical analyses, which led to a final test campaign on a prototype installed in real sea environment. Further developments are actually planned with the deployment of a larger prototype in a more energetic site. Given the great amount of tidal energy resource, the Strait of Messina is one of the most attractive areas in Italy for possible tidal device installations [1].

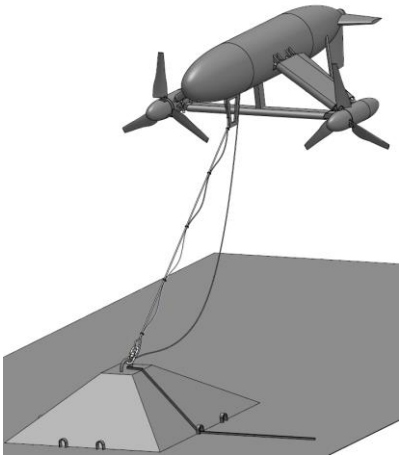

Fig. 1. GEMSTAR system general arrangement view.

II. MAIN CHARACTERISTICS OF THE SYSTEM

A. GEMSTAR system configuration

Table I reports the nomenclature used in the following sections.

This paper, with ID 1639, has been submitted in the EWTEC conference track "Tidal device development and testing".

D. P. Coiro is full professor at Department of Industrial Engineering, University of Naples "Federico II", via Claudio 21, Napoli, Italy (e-mail: coiro@unina.it).

G. Troise and N. Bizzarrini work at Seapower scrl, Via Giuseppe Fiorelli, 14, 80121, Napoli, Italy (e-mail: g.troise@seapowerscrl.com, n.bizzarrini@seapowerscrl.com).

G. Lazzerini cooperates with Department of Industrial Engineering, University of Naples " Federico II", via Claudio 21, Napoli, Italy (e-mail: guidolazzerini@gmail.com).

TABLE I. SYMBOLS

Symbol	Quantity	Unit
ρ	Density	kg/m³
v	Axial Velocity	m/s
a	Axial Induction	-
a'	Rotational Induction	-
N	Number of Blades	-
c	Section Chord	m
v_{rel}	Relative velocity	m/s
ω	Rotational velocity	rad/s
C_d	Sectional Drag Coefficient	-
C_l	Sectional Lift Coefficient	-
C_N	Normal Force Coefficient	-
C_H	Horizontal Force Coefficient	-
r	Section radius	m
R	Rotor Radius	m
dr	Radius increment between sections	m
dT	Thrust increment between sections	N
dP	Power increment between sections	W
T	Thrust	N
P	Power	W
α	Angle of attack	deg
θ	Sectional twist	deg
Φ	In-flow angle	deg
F_h	Sectional hydrodynamic force	N/m
L	Sectional lift	N/m
D	Sectional drag	N/m
N	Sectional normal force	N/m
H	Sectional horizontal force	N/m

Over the years, several concepts have been developed for the exploitation of tidal energy. The technical literature produced on this subject exhaustively highlights the main characteristics of such devices. A brief review of general considerations and possible device configurations, for instance, is provided by Vikas et al. [2] and by Roberts et al. [3].

The GEMSTAR exploits the kinetic energy of marine currents using hydrokinetic horizontal axis turbines. Looking at the connection to the seabed, unlike other hydro-turbines, which use a fixed or a gravity based foundation for the support structure, a moored floating support is used in this case, which can drastically reduce deployment and maintenance costs. GEMSTAR is, in fact, a tethered floating submerged system supporting two hydrokinetic turbines with self-alignment capability in reversing current regimes, as typically occurring in the case of tidal streams. The system may be equipped with a self-towing winch, which can set the system at the desired operating depth. Thanks to the underwater deployment, the GEMSTAR has a limited impact on navigation and other activities. The equilibrium at a proper working depth (with a suitable clearance with respect to seabed) is obtained thanks to the buoyancy of the main floating body and to the lift of the eventually wings if present, which balance the thrust acting on the turbines and the drag on the structures.

In order to control the device floating motion, a suitable mooring system is employed. Several mooring configurations are possible. In a basic arrangement, a single anchoring point on the seabed is used, allowing the rotation of the floating structure in response to the current direction changes. In the rest condition, the GEMSTAR system is set at a suitable depth under the water surface level and the mooring cable is positioned upright due to the action of the main body buoyancy. In presence of tidal currents, the system reaches an equilibrium condition due to the balance between buoyancy, system drag and turbines thrust, and the mooring cable forms an angle less than 90 degrees with respect to the seabed.

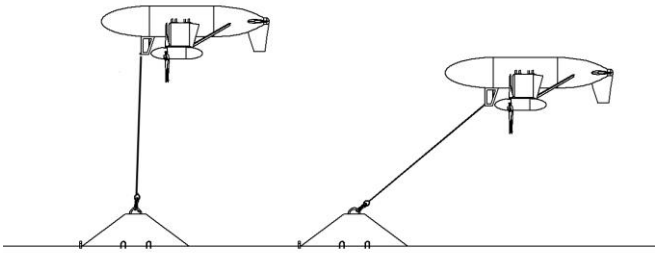

Fig. 2. GEMSTAR system operating conditions: at rest (left), under current action (right).

Other anchoring configurations are currently being investigated. In particular, an arrangement using multiple mooring cables is under development in order to reduce the needed buoyancy or the space occupation, or to increase the safety clearance. The system can be raised to the water surface, with the aim to carry out maintenance operations, by slowly releasing the mooring cable. In a possible configuration, currently at an early stage of conceptual development, a pressurization system can be used in order to change the effective buoyancy, with the aim to reduce the forces acting during the raising/lowering operations.

Two generators are installed on board and mounted on the turbine shafts through a gearbox. Each generator is electrically controlled by an inverter to allow grid connection and to track the optimal working conditions at different current speeds, by implementing a suitable control logic for rotational speed. The power connection is provided by means of a power cable, laid out along the mooring cable and extended up to an on-shore grid connection point.

B. GEMSTAR project development

Starting from the results obtained for the previously developed GEM system, the GEMSTAR project involves an extended series of research studies, including different sessions of experimental and numerical tests.

Research activities have partially been carried out at the University of Naples "Federico II" and a large-scale

prototype was also manufactured and installed in a relatively low-speed tidal stream site, in the Venice lagoon in 2012. The following table reports the different experimental set-ups for the main development stages.

Details on previous developments of the project and on the main results are described by Coiro *et al.* [4] [5]. However, the project is still in progress and a new test campaign on a larger rated power prototype is planned in the Strait of Messina, after a preliminary survey about the current resource and the geophysical characteristics in different possible deployment sites of interest.

TABLE II
GEMSTAR DEVELOPMENT HISTORY: EXPERIMENTAL TESTS ON DIFFERENT SCALE PROTOTYPES AND COMPONENTS

#	Tests	Dimensions and scale
1	Bare turbine (2005) (laboratory)	Rotor diameter: 1.20 m
2	Bare and shrouded turbines (2008-2010) (laboratory)	Rotor diameter: 0.6 m
3	Complete floating system (2010 - 2011) (laboratory)	Rotor diameter: 0.6 m (different configuration tested)
4	Full-scale prototype (2012) (sea environment)	Rotor diameter: 3 m

Various configurations of the system have been considered throughout its development. In particular, in the previous work, shrouded turbines were mounted with the aim of increasing the effective energy conversion efficiency (some observations on the shroud effect are reported, for instance, by Van Bussel [6] and Reinecke *et al.* [7]). A numerical analysis of the shroud effect is reported in [8]. The shroud is a toroidal shape component with an aerofoil section, placed around the turbine and acting as a diffuser. It is, in principle, able to largely increase the energy conversion efficiency; but, on the other hand, it also induces a considerable increase of the total frontal area and of the global thrust, as reported in [9]. Thereby, its economical effectiveness is still questionable for different applications. In the GEMSTAR system, the use of the shroud will be rejected in the configuration upgrade currently under development, in consideration of the following issues: cost increment due to the production of a complex shape component and additional structural holding members, thrust increment with a significant increase in required buoyancy and mooring system strength.

C. *Lab tests on a small-scale model (with bare turbines)*

The main results of the tests can be represented in terms of the non-dimensional power coefficient C_P defined by the following relation:

$$C_P = \frac{P}{\frac{1}{2}\rho V^3 S} \tag{1}$$

Where P is the output power, ρ is the water density, V is the current velocity and S is a reference surface, generally assumed equal to the turbine rotor disk area. The power coefficient is generally reported as a function of the tip speed ratio (TSR), defined as the ratio of the turbine peripheral speed ΩR to the flow asymptotic velocity:

$$TSR = \frac{\omega R}{V} \tag{2}$$

where ω is rotational speed and R is the rotor radius.

The measured bare turbine power coefficient, based on mechanical shaft power, is reported in Fig. 3. The results were obtained through experimental tests on a small-scale model of the whole GEM floating system, carried out in the towing tank of the University "Federico II".

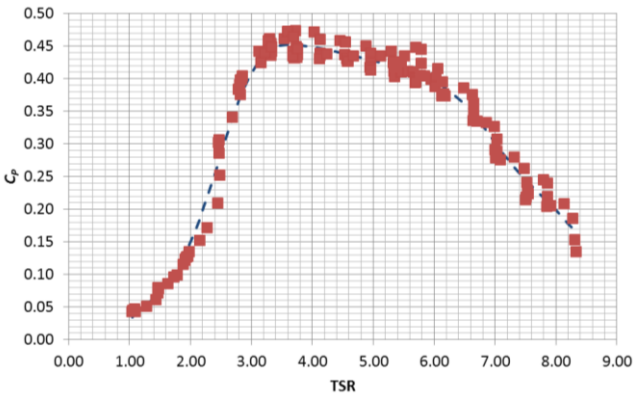

Fig. 3. Power coefficient of a bare turbine mounted on the GEM floating system model (towing tank tests). Red dots are the experimental measurements and the dotted line represents cubic-spline fitting.

A maximum power coefficient value of about $C_{Pmax} = 0.45$ can be observed at approximately $TSR = 4$. Such figures can be used to estimate the required dimensions of a device for a desired rated power.

A further electromechanical efficiency, η, has to be applied to the hydrodynamic power coefficient:

$$\eta = \eta_m \eta_e = 0.81 \tag{3}$$

where η_m and η_e respectively represent the mechanical and electrical losses.

D. *Sea environment tests on a large-scale model (with shrouded turbines)*

A large-scale model was manufactured and deployed in a site of the Venice lagoon, where a relatively low maximum current speed (about 1.5 m/s) is present. A picture of the prototype is shown in Fig. 4 and it was partially financed by Veneto regional Authority.

Fig. 4. First GEM prototype on the dock.

The device rated power was about 20 kW at the local maximum current speed.

Fig. 5 shows the turbines (left and right) power curves (nondimensionalized with respect to the maximum measured power peak) as a function of current speed referred to the peak velocity.

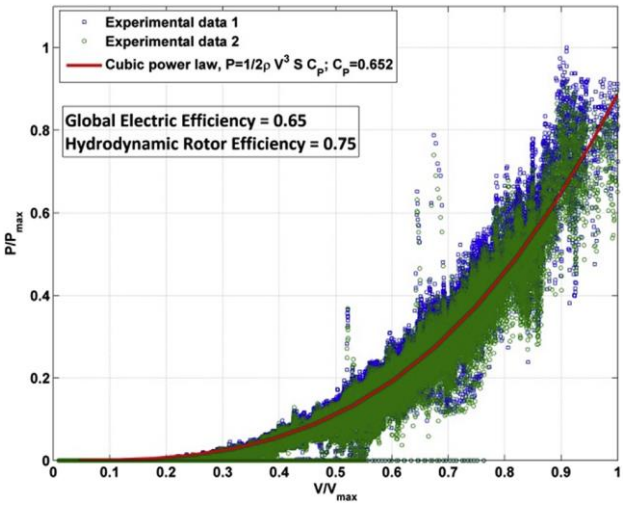

Fig. 5. Normalized power curves of the shrouded turbines mounted on the GEM large-scale prototype (sea environment tests).

The power production has been evaluated by measuring the electrical power output together with the current speed, measured by means of an ADCP (Acoustic Doppler Current Profiler) sensor, which allows the estimation of the flow velocity along a water column from surface to seabed.

A control system was used to track the optimal power generation conditions, keeping an almost constant TSR, until rated power. An almost cubic variation of power output with current speed can be observed.

Fig. 5 also shows an experimental estimation of the power coefficient, obtained by fitting a cubic law to the measured data of power and speed.

The overall electrical power coefficient is approximately equal to 0.65, accounting also for electrical conversion losses at generator output. The mechanical power coefficient (accounting only for the hydrodynamic conversion efficiency at rotor shaft) may be estimated assuming typical values for mechanical and electrical efficiencies. Considering an electrical efficiency of about ~0.9 and a mechanical efficiency of about ~0.9, a mechanical power coefficient roughly equal to 0.75 – 0.8 can be estimated, which is comparable with the results obtained in previous lab tests on the shrouded turbine and on the GEM small-scale model.

III. TURBINE BLADE DESIGN

E. Control strategy definition

In order to exploit the maximum available energy, it may be considered a device with cut-out speed equal to or slightly greater than the maximum speed expected in the installation site. Once the generator size is chosen, a proper control strategy must be implemented in order to avoid excessive power output at flow speeds above the nominal value. Several control schemes are possible. The approach considered at the actual stage of the project development applies an overspeed strategy. In the considered solution, the use of a de-fluxing technique is assumed in order to require a constant power output above the nominal current speed. Essentially, through this approach, the constant power condition is attained by reducing the required torque while increasing the rotational speed of the generator. Further details on this control method are given in [10].

The choice of such a strategy requires a specific design of the blade in order to fulfil the following requirements in the above rated operating regime (between the nominal and the cut-out current speeds):

a) limiting the increase of rotational speed in order to avoid cavitation phenomena, to reduce centrifugal forces and to make the generator work within a suitable rpm range (the maximum rpm has been established to be twice its rated value);
b) limiting power output and thrust variations (both have been fixed to be equal to their rated value).

Both these conditions have an influence on the design of the turbine blade, which is the subject of the following sections.

F. Blade shape definition

Marine environment, in which the GEMSTAR system works, is generally characterized by a relatively predictable behaviour, particularly in the case of tidal currents, allowing for a more confident definition of the maximum operating conditions. Moreover, in general, turbulence velocity fluctuations are more limited in comparison to the atmospheric environment. Thus, the specific environmental conditions reduce the need for a responsive and expensive active pitch control system, as in the case, for example, of wind turbines, offering the chance to adopt a fixed pitch design, avoiding movable parts that lead to higher costs.

In this case, the power output is controlled by varying the rotational speed in order to maximise the power output under the nominal current speed and to limit the power output at higher speeds.

More specifically, at flow speeds under the nominal value, the control system varies the rotational speed in order to maintain a constant value of TSR, corresponding to the maximum CP. In this region, the control system tracks the optimal power coefficient and the power output increases following a typical cubic curve (CP being constant).

At the rated current speed, the maximum generator power is reached. Above this condition, the control system increases the rotational speed in order to keep a constant value of power output.

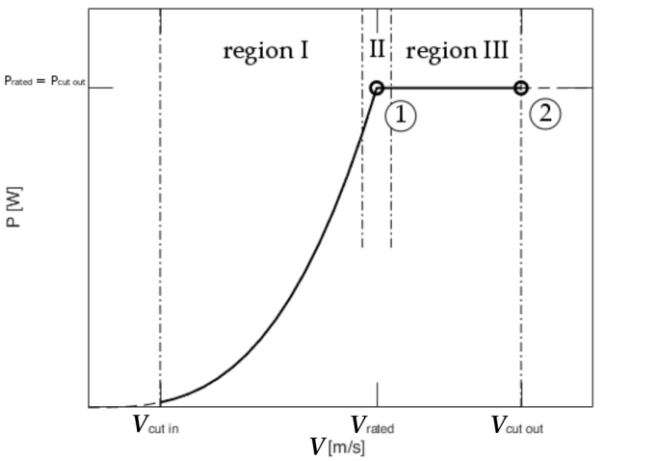

Fig. 6. Ideal rotor power output curve, the circled numbers represent the two operating conditions, the other numbers represent the operating ranges. The power output increases as the cube of the stream speed in **I**, reaches the maximum value in **II**, and it is kept constant in **III**.

Thereby, assuming the maximum value of the stream speed, we need to ensure that the rotor mechanical power output is constant in the operating range between the rated and the cut-out velocity, trying not to exceed the maximum allowable power input at the electrical generator.

A design procedure has been implemented so that the power output and the thrust are the same for two different operating conditions, the first being the nominal operating condition, and the second being the operating condition with the maximum current speed.

This constraint can be expressed in terms of the sectional thrust and power distribution along the turbine's blade span.

Following the Blade Element Momentum (BEM) theory as in [11], one can express the sectional thrust and power as:

$$dT = \rho V^2 4a\,(1-a)\,\pi\, r dr = \frac{1}{2} N\, c\, \rho {V_{rel}}^2\, C_N\, dr \tag{7}$$

$$dP = \rho V\, \omega^2 a'(1-a) 4\pi r^3 dr = \omega \frac{1}{2} N\, c\, \rho\, {V_{rel}}^2 C_H r\, dr \tag{8}$$

where the symbols are explained in Table I and a visual representation of the quantities is given in figure 7 and 8.

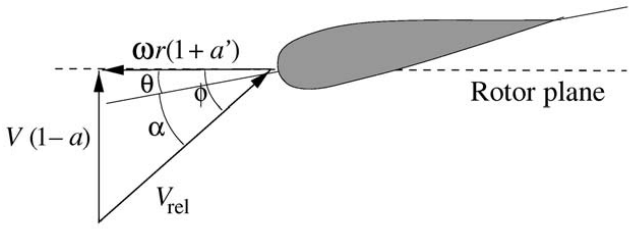

Fig. 7. Relative velocity with axial and rotational inductions at a section of the rotor blade (Reproduced from [11]).

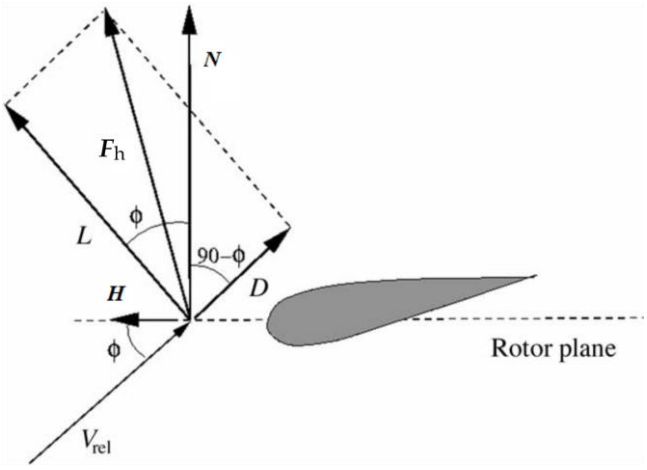

Fig. 8. Hydrodynamic forces on a section and the normal and parallel projections with respect to the rotor plane (Reproduced from [11]).

For the power and the thrust to be constant at two operating conditions, say condition 1 and condition 2, we impose the same sectional contribution:

$$dT_1 = dT_2 \tag{9}$$

$$dP_1 = dP_2 \tag{10}$$

which, for the expressions of the thrust and power given by the disk actuator theory, becomes:

$$\rho {V_1}^2 4a_1(1-a_1)\pi r dr = \rho {V_2}^2 4a_2(1-a_2)\pi r dr \tag{11}$$

$$\rho V_1 \omega_1^2 a_1'(1-a_1) 4\pi r^3 dr = \rho V_2 \omega_2^2 a_2'(1-a_2) 4\pi r^3 dr \tag{12}$$

The unknown axial and rotational inductions and the sectional hydrodynamic coefficients will be then computed from equations 7 and 8 coupled with equations 11 and 12 to match the desired constraints.

We get the following system (where equations 7, 8, 11 and 12 have been simplified):

$${V_1}^2 8a_1(1-a_1)\pi r = N_B c\, {V_{rel,1}}^2 \left(C_{l,1} cos(\phi_1) + C_{d,1} sin(\phi_1)\right) \tag{13}$$

$$V_1\omega_1^2 8a_1'(1-a_1)\pi r^2 = N_B\, c\, {V_{rel,1}}^2\big(C_{l,1}\, sin(\phi_1) - C_{d,1}\, cos(\phi_1)\big) \quad (14)$$

$${V_2}^2 8a_2(1-a_2)\pi r = N_B c\, {V_{rel,2}}^2\big(C_{l,2}\, cos(\phi_2) + C_{d,2}\, sin(\phi_2)\big) \quad (15)$$

$$V_2\omega_2^2 8a_2'(1-a_2)\pi r^2 = N_B\, c\, {V_{rel,2}}^2\big(C_{l,2}\, sin(\phi_2) - C_{d,2}\, cos(\phi_2)\big) \quad (16)$$

$${V_1}^2 a_1(1-a_1) = {V_2}^2 a_2(1-a_2) \quad (17)$$

$$V_1\omega_1^2 a_1'(1-a_1) = V_2\omega_2^2 a_2'(1-a_2) \quad (18)$$

The variables are a_1, a_2, a_1', a_2', and the lift coefficients at the two operating conditions. For any given sectional hydrofoil, the hydrodynamic coefficients, that can be found as $C_l(\alpha)$ and $C_d(C_l)$ functions, must be calculated altogether with the equations presented above. For both the 2-D lift coefficient and drag coefficient we use a spline interpolant of the curves calculated with the well-known XFOIL software [12]. We add the equation that links the two operating condition's lift coefficients:

$$C_{l,2} - C_{l,1} = C_{l_\alpha}\Delta\alpha \quad (19)$$

The solution of the system of equations becomes impossible because the variables are six (four inductions plus two lift coefficients) but the system is composed of seven equations. So, one can decide to let the drag coefficient at the second operating condition be the seventh variable and try to match it later, section by section, with an appropriate hydrofoil.

A Newton-Raphson method can be used to solve for the unknown quantities and then calculate the sectional angle of attack which gives the desired lift coefficient with an inverse function $\alpha(C_l)$. Through the angle of attack α and the inflow angle φ we obtain the desired sectional twist angle θ distribution as follows:

$$\theta(r) = \phi(r) - \alpha(r) \quad (20)$$

The twist distribution calculated through this analytical procedure has been assigned to the geometry of the rotor and the performance of this new geometry has been analysed with the software WTPerf [13]. Due to the simple analysis employed in the system of equations and the neglecting of other effects, such as Prandtl tip losses, differences are expected with respect to the numerical results obtained using WTPerf. The chord distribution is calculated through the Glauert's optimization as in [11], choosing the first operating condition as the design point. To simplify the problem, a single hydrofoil has been chosen along the blade span and the Reynolds number used for hydrodynamic coefficients is $5 * 10^6$.

The design of the rotor blades must take into account the effects of cavitation, that is the generation of vapour bubbles when the local pressure of the fluid is lower than the vapour pressure, that is a function of the fluid itself and temperature. To avoid and limit the formation of such bubbles, the pressure reduction on the blade generated by the expansion of the fluid must be small at the operating conditions. This constraint must be accounted for when the pressure distribution on the blade at the operating condition is calculated, through the limitation of the negative peak of the pressure coefficient.

In a first attempt, an hydrofoil specifically designed to avoid cavitation phenomena has been adopted; nevertheless, the hydrodynamic characteristics of the hydrofoil have not allowed to comply with the imposed constraints on power and thrust at the operating conditions 1 and 2. Therefore, Eppler 818 hydrofoil has been chosen for the blade optimization procedure reported in this paper. Such hydrofoil exhibits a decrease of efficiency, passing from condition 1 to condition 2, able to maintain a constant value of power and thrust but still insufficient to reach all desired goals. A new specific hydrofoil is currently being designed to better match the constraints imposed by the desired requirements. The operating conditions and the rotor geometry are summarized in table III and IV.

TABLE III
OPERATING CONDITIONS

Operating Condition	Current Speed	Rotor Speed
1	2 m/s	16 RPM
2	3 m/s	32 RPM

TABLE IV
ROTOR GEOMETRY

Rotor radius	6 m		
Hub radius	0.6 m		
N° of blades	3		
Chord distribution	Glauert's theory optimization, design point 1	Glauert's theory optimization design point 1 - chord increased.	Genetic algorithm optimization
Hydrofoil	EPPLER E818		

The system solution leads to a desired output of the drag coefficient at the operating condition 2, as shown in Fig.9, in which the values of real hydrofoil Cd (at same lift coefficients) seem to be constant along the blade span, but this is due not only to the figure scale effect but also to the small differences between the different sectional lift coefficients as shown in Fig.10.

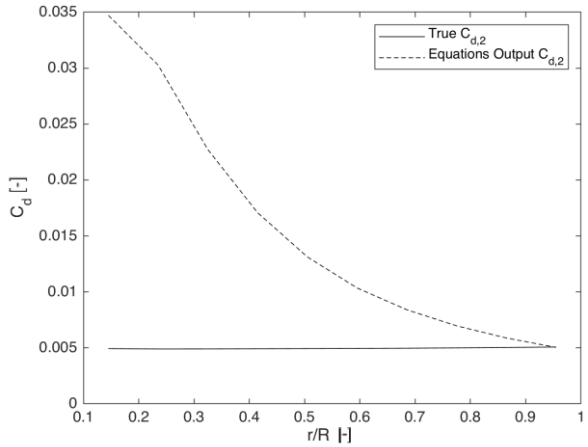

Fig. 9. Sectional drag coefficient estimation at the second operating condition.

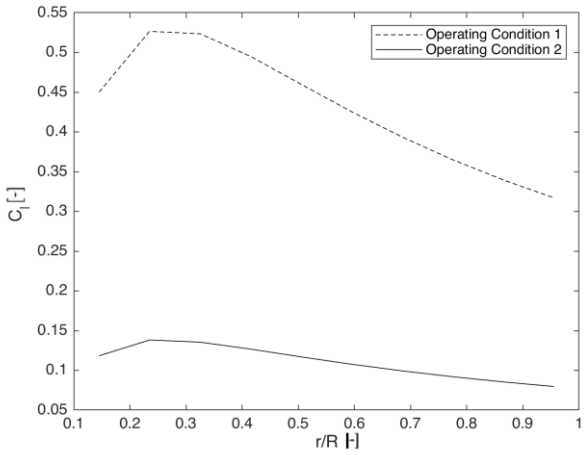

Fig. 10. Sectional lift coefficient estimation at the two operating conditions.

It can be observed that significant differences exist, especially in the inboard part of the blade, between the "desired" and real hydrofoil Cd values indicating limited prospect in obtaining the desired performances.

Table V reports the power and thrust values of the new rotor blade, analysed in conditions 1 and 2, through the simplified analytical procedure previously discussed and using WTPerf.

TABLE V. PERFORMANCE OF THE TURBINE WITH THE TWIST ANGLE DISTRIBUTION MODIFIED BY THE ALGORITHM.

Operating Condition	P Analytical procedure	P WTPerf	T Analytical procedure	T WTPerf
1	135.7 kW (Cp = 0.29)	127 kW (Cp = 0.27)	82.1 kN	78 kN
2	135.7 kW (Cp = 0.09)	166 kW (Cp = 0.11)	82.1 kN	78.4 kN

It can be noticed that, as expected, there are some discrepancies between the simplified analytical procedure and WTPerf, especially in the estimation of the power output. More specifically, according to WTPerf results, the power is not constant but, at the second operating condition, it becomes approximately 30% higher than the power at the first operating condition. This is due to the difference between the desired drag coefficient at the second operating condition and the real hydrofoil drag coefficient and some physical phenomena that are taken into account in WTPerf but neglected in the analytical procedure (i.e. Tip Losses, etc).

Moreover, if we compare the power output at the operating condition 1 with the one produced by the same chord with the twist distribution optimized through Glauert's theory for the nominal current speed (around 220 kW), we notice that the loss is around 40%. This is obviously due to the twist distribution given as output of the equations system, which is not optimized according to the Glauert's theory.

The comparison between the power coefficient and the thrust coefficient curves generated by the two different rotor twist design are shown in Fig. 11 and Fig. 12. The power coefficient of the geometry optimized through Glauert's theory shows a higher value of the power coefficient at the operating condition 1, but it is inevitably unsuitable for the purpose of limiting the power output at the operating condition 2.

The curves generated by the rotor twist designed to accomplish the equivalence of power and thrust outputs at the two conditions show lower maxima of both power and thrust coefficients but steeper curves slope that account for decreasing the outputs at the operating condition 2.

A first attempt of chord modification, keeping the same twist distribution, was carried out to increase the power output while maintaining the desired requirements. The related results are reported in the table below.

TABLE VI
PERFORMANCE OF THE TURBINE WITH THE TWIST ANGLE DISTRIBUTION MODIFIED BY THE ALGORITHM AND CHORD DISTRIBUTION INCREASED BY 50%

Operating Condition	P Analytical procedure	P WTPerf	T Analytical procedure	T WTPerf
1	164.2 kW (Cp = 0.35)	152.4 kW (Cp = 0.33)	103.9 kN	98.0 kN
2	164.2 kW (Cp = 0.11)	186.7 kW (Cp = 0.12)	103.9 kN	98.0 kN

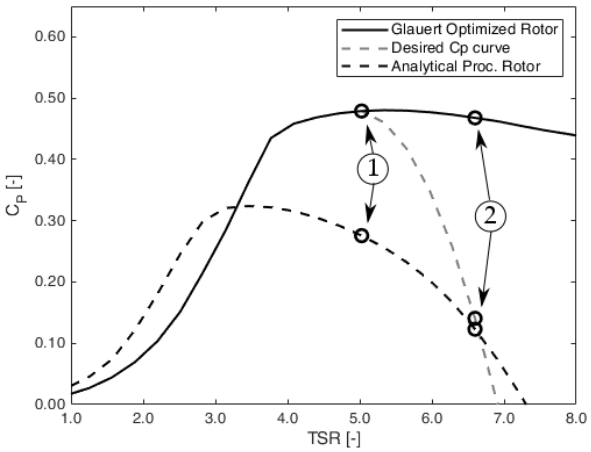

Fig. 11. Power coefficient curves of the two rotors with different twist and the desired curve (dashed line in grey), the circles represent the values corresponding to the first and second operating conditions.

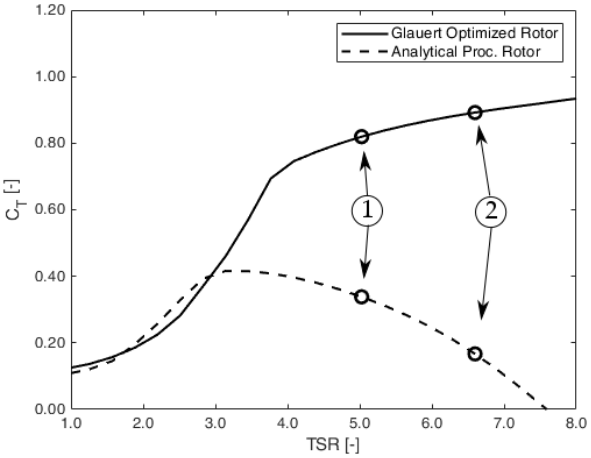

Fig. 12. Thrust coefficient curves of the two rotors with different twist, the circles represent the values corresponding to the first and second operating conditions.

The increased chord configuration shows a power output increased by about 20% with respect to the chord optimized for the nominal current speed, and the thrust output is 25% higher; however the power coefficient at the operating condition 1 is still considerably lower than the desired one, as shown in Fig. 13.

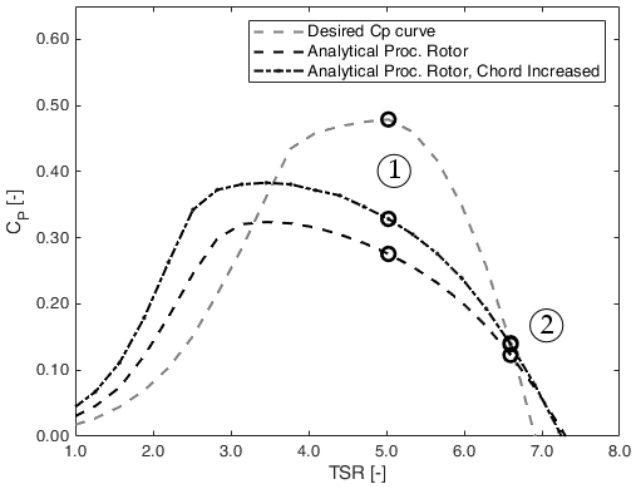

Fig. 13. Power coefficient curves of the two rotors with different chord and the desired curve (dashed line in grey), the circles represent the values corresponding to the first and second operating conditions.

The combined effects of chord and twist distribution variation have been investigated through a genetic algorithm multi-objective optimization. The flowchart of the algorithm is shown in Fig. 14.

The variables of the design space were the values of the chord and twist at five control points along the blade span, then the chord and twist distribution were re-created through interpolation with piece-wise cubic splines. The multi-objective function consisted of the mechanical power output at first operating condition, the difference between the mechanical power outputs at the first and second operating conditions and the difference between the thrust outputs at the first and second operating conditions.

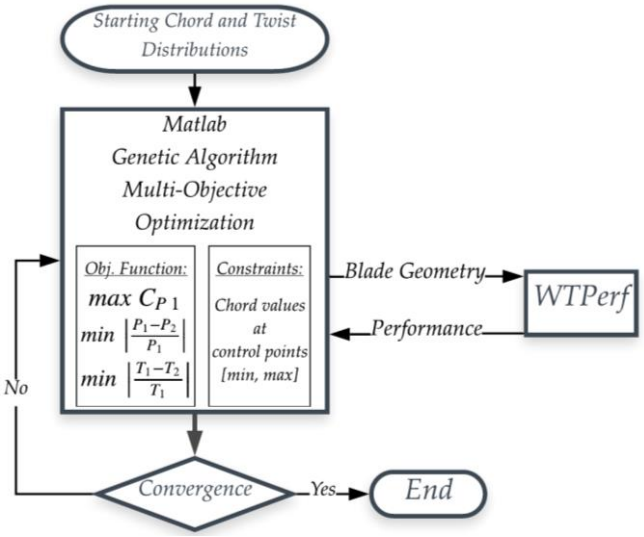

Fig. 14. Flow-chart of the optimization tool with the integration of the Matlab genetic algorithm and WTPerf.

The integrated Matlab multi-objective genetic optimization tool, of which the theoretical background can be found in [14], was employed and integrated with the software WTPerf that evaluates the hydrodynamic performance of each individual.

Each generation created by the tool consisted of 200 individuals (each one representing a rotor blade geometry). A convergence parameter based on the average distance, called "spread", between the selected individuals of the last generation and the selected individuals of the past generations, namely the *Pareto Front*, was chosen to stop the iterations. The optimization tool stopped after 118 generations.

The performance of the individual with the highest power output value at the first operating condition, with the difference in both power and thrust outputs being less than 5% is shown in Table VII, whereas the chord and twist distributions, compared to those obtained with the analytical procedure, is plotted in Fig. 15 and Fig. 16.

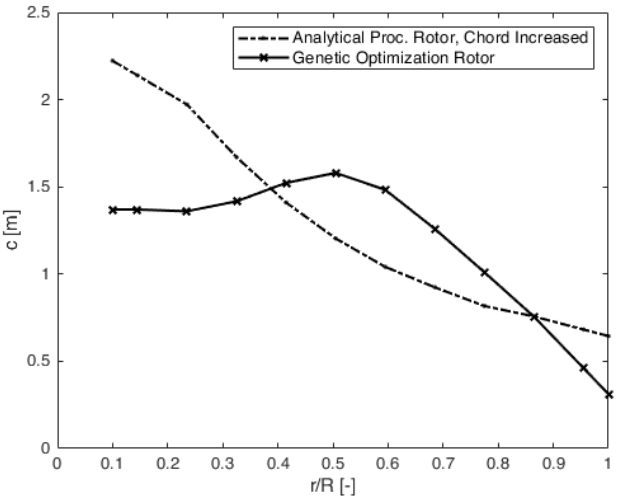

Fig. 15. Comparison between the chord distribution used in the analytical procedure and the one obtained through the optimization tool.

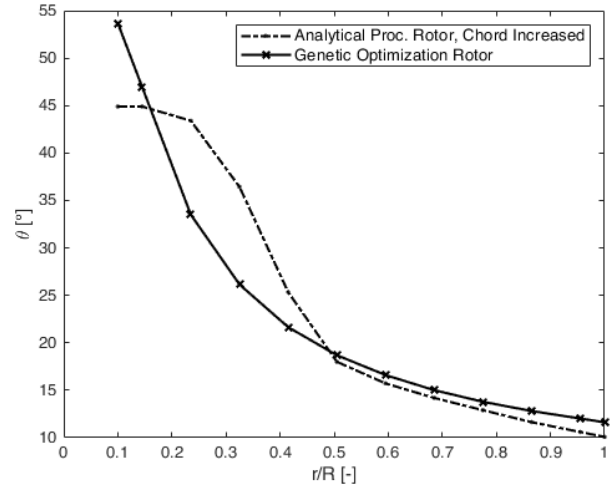

Fig. 16. Comparison between the twist distribution obtained through the analytical procedure and the one obtained through the optimization tool.

TABLE VII. PERFORMANCE OF THE TURBINE WITH THE CHORD AND THE TWIST ANGLE DISTRIBUTIONS MODIFIED BY THE GENETIC OPTIMIZATION ALGORITHM.

Operating Condition	P WTPerf	T WTPerf
1	149.0 kW (Cp = 0.32)	100.0 kN
2	146.4 kW (Cp = 0.09)	99.7 kN

The power and thrust coefficients curves are compared with those coming from the analytical procedure in Fig. 17 and Fig. 18.

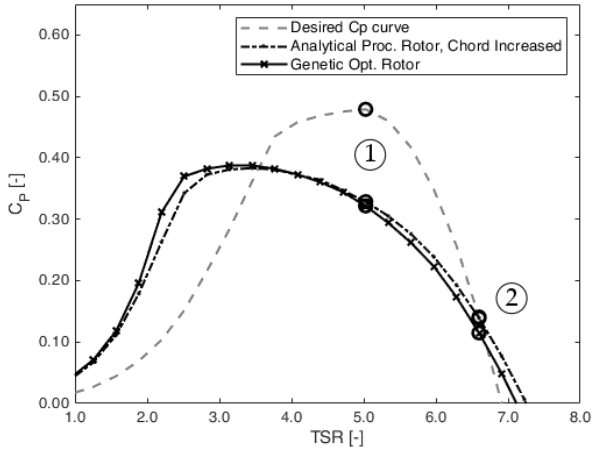

Fig. 17. Power coefficient curves of the two rotors with different design approach and the desired curve (dashed line in grey), the circles represent the values corresponding to the first and second operating conditions.

It can be noticed that the shapes of the curves generated by the rotors obtained through the analytical procedure and the optimization tool do not differ significantly confirming the reliability of the fast analytical solution despite the differences in chords distribution along blade span. Furthermore, the power and thrust coefficients values corresponding to the two operating conditions are similar; the similarity of the results of the two approaches suggests that a future development to improve the performance of the rotor maintaining the desired requirements must include the design of a specific hydrofoil.

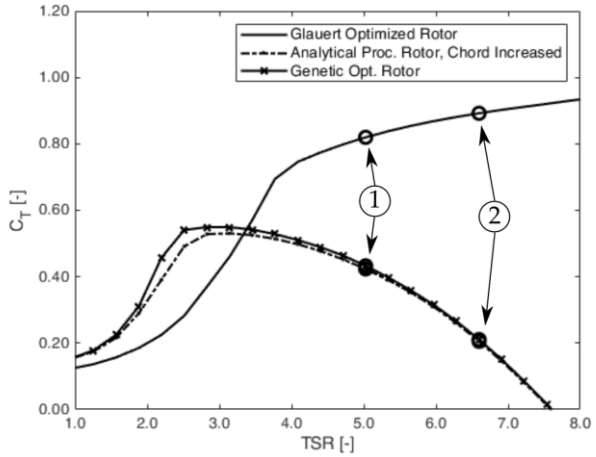

Fig. 18. Thrust coefficient curves corresponding to the rotors obtained with the two design approaches and to the Glauert optimized rotor; the circles represent the values corresponding to the first and second operating conditions.

IV. CONCLUSIONS

The main results of numerical and experimental studies carried out for the development of the GEMSTAR system have been reported. The last improvements applied to the system in order to reduce the weight and the manufacturing costs, while keeping satisfactory power performance, have been presented. In particular, the choice of removing the shrouds has been justified, a new power control strategy for fixed pitch rotor and the requested redesign of the turbine blades, with its effect on the power output and the thrust, have been presented. Through the new blade optimization, a suitable geometry has been obtained, which is able to satisfy the desired requirements: almost constant values of power and thrust at current speeds over the nominal value, and maximum rotational speed limited to twice its rated value. Further improvements are needed in order to increase the maximum value of efficiency.

REFERENCES

[1] D. P. Coiro, G. Troise, C. Ciuffardi e G. M. Sannino, «Tidal current energy resource assessment: the Strait of Messina test case,» in *International Conference on Clean Electrical Power : Renewable Energy Resources Impact DOI: 10.1109/ICCEP.2013.6586992*, Alghero, Italy, 2013.

[2] M. Vikas, S. Rao and J. K. Seelam, "Tidal Energy: a review," in *Proceedings of International Conference on Hydraulics, Water Resources and Coastal Engineering (Hydro2016)*, Pune, India, 2016.

[3] A. Roberts, B. Thomas, P. Sewell, Z. Khan, Z. Balmain and J. Gillman, "Current tidal power technologies and their suitability for applications in coastal and marine areas," *J. Ocean Eng. Mar. Energy*, 2016.

[4] D. P. Coiro, G. Troise e F. Scherillo, «Design, towing tank test and deployment of full scale GEM, a novel tethered system for harnessing tidal energy,» in *Proceeding of Asian Wave and Tidal Energy Conference (AWTEC 2012)*, Jeju (South Corea), 2012.

[5] D. P. Coiro, G. Troise and N. Bizzarrini, "Experiences in Developing Tidal Current and Wave Energy Devices for Mediterranean Sea," *Frontiers in Energy Research,* vol. 6, no. DOI 10.3389/fenrg.2018.00136, p. 136, 12 December 2018.

[6] G. J. Van Bussel, «The science of making more torque from wind: Diffuser experiments and theory revisited.,» *Journal of Physics,* pp. 1-12, 2111 2007.

[7] J. Reinecke, T. Von Backstrom e G. Venter, «Effect of a Diffuser on the Performance of an Ocean Current Turbine,» in *9th European Wave and Tidal Energy Conference, (EWTEC)*, 2011.

[8] E. Daniele, E. Ferrauto e D. P. Coiro, « "Horizontal Axis Hydroturbine Shroud Hydrofoil Optimization",» *Advances in Evolutionary and Deterministic Methods for DesignOptimization and Control in Engineering and Sciences,* n. 36, pp. pp. 241-256., 2014.

[9] F. Scherillo, G. Troise, D.P.Coiro and S. Miranda, "Numerical and experimental Analysis of a Strouded Hydroturbine," in *ICCEP Conference*, Ischia,Italy, June 2011, DOI: 10.1109/ICCEP.2011.6036277.

[10] Z. Zhou, F. Scuiller, J. F. Charpentier, M. E. H. Benbouzid e T. Tang, «Power Control of a Nonpitchable PMSG-Based Marine Current Turbine at Overrated Current Speed With Flux-Weakening Strategy,» *IEEE JOURNAL OF OCEANIC ENGINEERING,* n. DOI: 10.1109/JOE.2014.2356936, 2014.

[11] M. O. L. Hansen, Aerodynamics of Wind Turbines, London: Earthscan, 2008.

[12] M. Drela, "XFOIL: An Analysis and Design System for Low Reynolds Number Hydrofoils," in *Proceedings of the Conference Low Reynolds Number Aerodynamics*, Notre Dame, Indiana, USA, 1989.

[13] A. D. Platt e M. L. Buhl Jr., WT_Perf User Guide for Version 3.05.00, Golden, CO: NREL (National Renewable Energy Laboratory), 2012.

[14] MathWorks, "Matlab R2018b Documentation," MathWorks, 2018. [Online]. Available: https://it.mathworks.com/help/gads/gamultiobj.html. [Accessed 14 January 2019].